



# Vibration-induced mobilization of trapped oil ganglia in porous media: Experimental validation of a capillary-physics mechanism

Wenqing Li<sup>a</sup>, R. Dennis Vigil<sup>a,\*</sup>, Igor A. Beresnev<sup>b</sup>, Pavel Iassonov<sup>b</sup>, Robert Ewing<sup>c</sup>

<sup>a</sup> Department of Chemical Engineering, Iowa State University, 2114 Sweeney Hall, Ames, IA 50011-2230, USA

<sup>b</sup> Department of Geological and Atmospheric Sciences, Iowa State University, 253 Science I, Ames, IA 50011-3212, USA

<sup>c</sup> Department of Agronomy, Iowa State University, 2101 Agronomy Hall, Ames, IA 50011, USA

Received 11 January 2005; accepted 20 March 2005

Available online 30 April 2005

## Abstract

The development of methods for mobilizing residual organic liquids trapped in porous media is becoming increasingly important as world demand for oil increases and because of the need to remediate aquifers degraded by slow-dissolving organic contaminants. Low-frequency elastic wave stimulation is one such technique, but until recently the lack of a mechanistic understanding of the effects of vibration on mobilization of oil ganglia has prevented the method from being applied predictably in the field. Recently, a simple capillary-physics mechanism has been developed to explain vibration-induced mobilization of a trapped non-wetting organic phase in porous media. Specific predictions that follow from this hypothesized mechanism are that vibrations will be most effective in mobilizing trapped oil when the acceleration amplitude is within an optimal range of values (that depend on the magnitudes of the capillary forces trapping the ganglia and the imposed static pressure gradients) and for sufficiently low vibration frequencies. In this paper we describe two-dimensional glass micromodel experiments that support these predictions.

© 2005 Elsevier Inc. All rights reserved.

**Keywords:** Elastic wave stimulation; Multiphase flow; Porous media; Acoustic stimulation; Enhanced oil recovery; Non-aqueous phase liquids

## 1. Introduction

Multiphase flow in porous media is a complicated and incompletely understood problem with important practical applications to enhanced oil recovery, environmental remediation, and chemical reaction engineering. A common feature of these systems is the capillary entrapment of disperse phase ganglia in small pores. For aqueous-organic liquid-liquid systems, several strategies for mobilizing residual oil in porous media have been proposed, including using water flooding [1], adding surfactants to lower interfacial surface tension [2–4], increasing oil dissolution with co-solvents [5,6], using electro-osmosis [6,7], and irradiating the medium with elastic waves [8–10]. Several investigators

have studied the use of ultrasonic waves to enhance the transport of a trapped oil phase in water, but this method requires high intensity irradiation to be effective, and even then it typically works well only for ranges less than a meter from the acoustic actuator, thereby rendering it impractical for use on the field scale [11].

Because of the limitations of ultrasonic irradiation, interest in elastic wave stimulation (EWS) has become focused on low-frequency irradiation, which does not suffer from attenuation over short length scales. Beresnev and Johnson [8] have provided a comprehensive review of methods and results for both laboratory experiments and field case studies using EWS. However, despite the existence of some early studies and anecdotal evidence, such as changes in oil field productivity during earthquakes, well-controlled experiments that quantitatively demonstrate the efficacy of low-frequency EWS on ganglia mobilization have been lacking.

\* Corresponding author. Fax: +1 515 294 2689.

E-mail address: [vigil@iastate.edu](mailto:vigil@iastate.edu) (R.D. Vigil).

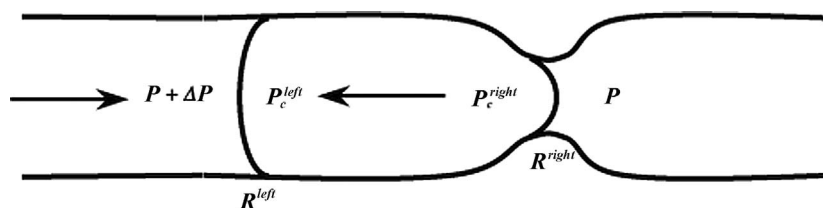


Fig. 1. Schematic of droplet flow through a horizontal straight channel with a constriction under a static pressure gradient  $\Delta P$ . The radii of the trailing and leading droplet menisci are labeled as  $R^{\text{left}}$  and  $R^{\text{right}}$ , respectively (as shown,  $R^{\text{left}} > R^{\text{right}}$ ). The corresponding internal capillary pressures are given by  $P_c^{\text{left}}$  and  $P_c^{\text{right}}$ .

Progress has also been limited by the absence of a validated pore-scale mechanistic explanation for ganglia transport enhancement.

Recently I.A. Beresnev, W.D. Pennington, and R.M. Turpening, building on numerical simulations by Graham and Higdon [12] and Iassonov and Beresnev [13], have articulated a simple capillary-physics mechanism to explain ganglia mobilization by low-frequency vibrations by considering the behavior of a single non-wetting droplet trapped at the entrance to a constriction in a tubular channel, as illustrated in Fig. 1. The most salient feature of this constricted pore geometry is that an excess capillary pressure is built on the internal side of the downstream meniscus as the droplet enters the pore constriction because the radius of the left (upstream) meniscus  $R^{\text{left}}$  is greater than the radius of the right meniscus  $R^{\text{right}}$ . Hence, an internal capillary-pressure imbalance  $P_c^{\text{right}} - P_c^{\text{left}}$  is created that resists the external gradient. As the droplet moves toward the narrowest part of the constriction, this capillary-pressure imbalance increases. However, before this maximum capillary imbalance is reached, the droplet will become trapped if  $P_c^{\text{right}} - P_c^{\text{left}}$  becomes sufficiently large that it equals the driving static external pressure gradient,  $\Delta P_s$ . In such cases, the external gradient must be increased above an unplugging threshold,  $\Delta P_0$ , in order for the droplet to pass through the constriction.

In view of these considerations, the expected average flow rate as a function of external pressure gradient is shown in Fig. 2. The expectation is that no flow occurs (and the droplet will be trapped) unless the static gradient  $\Delta P_s$  exceeds  $\Delta P_0$ . As  $\Delta P_s$  is increased from zero to  $\Delta P_0$ , only the equilibrium position of the trapped droplet changes (such that the resisting capillary-pressure imbalance is identical in magnitude to  $\Delta P_s$ ). For values of  $\Delta P_s$  greater than the unplugging threshold, the flow would be expected to follow the Darcy law.

If the static external gradient  $\Delta P_s$  is below the unplugging threshold  $\Delta P_0$  and a longitudinal vibration of the wall parallel to the pore axis is applied, an inertial force  $P_{\text{osc}}$  on the fluid will be induced with the amplitude of approximately  $\rho_f a_0$ , where  $\rho_f$  is the average density of the fluid and  $a_0$  is the acceleration amplitude of the wall [14]. The instantaneous total combined positive force on the fluid then becomes  $P_{\text{osc}} + \Delta P_s$ . One cycle of this combined force is shown on a vertical scale in Fig. 2 for an acceleration amplitude sufficiently large so that  $P_{\text{osc}} + \Delta P_s$  exceeds  $\Delta P_0$

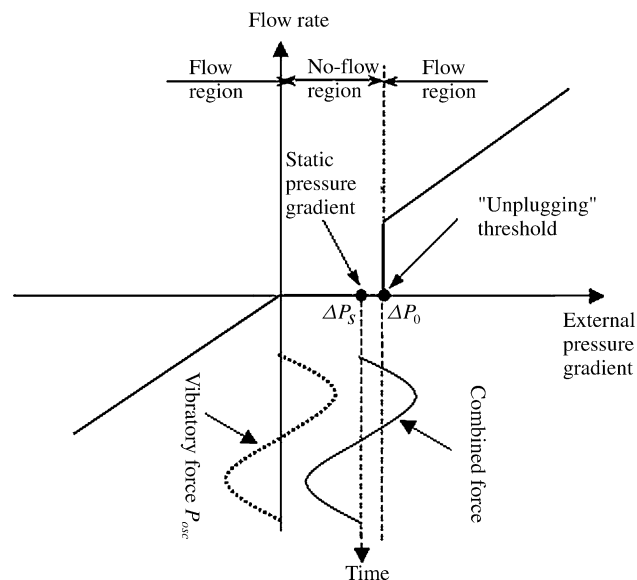


Fig. 2. Average flow rate as a function of the combined static pressure and vibratory pressure, explaining the mobilization mechanism.

during part of the vibration cycle. In the positive half-period of vibrations, when the total forcing exceeds  $\Delta P_0$ , the ganglion is instantly unplugged and moves forward, whereas, when the vibration reverses direction, the ganglion is once again plugged. Consequently a rectification effect occurs, leading to a “nudging” motion of the ganglion through the constriction in the positive half-cycles. After a number of cycles, the ganglion is mobilized.

At least two specific predictions based on this mobilization mechanism follow. First, for a fixed vibration frequency, the effect will grow with increasing acceleration amplitude of vibrations, which will simply increase the amplitude of  $P_{\text{osc}}$ . However, as the acceleration amplitude continues to increase, eventually no further ganglia mobilization will be realized as the negative half-cycles of each vibration will begin sampling large parts of the negative flow portion of the flow curve in Fig. 2 and the system will conform to the usual Darcy flow. Second, the net displacement of the ganglion over one period of vibrations will depend on how much time it spends in the unplugged position. For constant acceleration amplitude, therefore, the effect will be inversely proportional to the frequency. Furthermore, for sufficiently large frequencies, the vibrations will become ineffectual as the ganglia response time becomes large compared to the vibra-

tion period. The ganglion response time, sometimes called the “viscous diffusion time,” is the characteristic time scale over which the fluid responds to a step forcing,  $\tau = \rho_f r^2 / \mu$ , where  $r$  is the radius of the pore channel and  $\mu$  is the dynamic viscosity [15].

The purpose of this study is to validate these predictions using a two-dimensional etched-glass micromodel.

## 2. Experimental apparatus and protocol

An etched glass quasi-two-dimensional micromodel, a shaker, and a digital camera were used to study the effects of external vibration on the transport of oil ganglia in a water-flooded pore network. The horizontally mounted micromodel consists of a  $50 \times 50$  square lattice of circular “pores” connected by straight channel “throats,” as shown in Fig. 3. The non-uniform pore and throat diameters are approximately normally distributed and have mean values of 2.30 and 0.76 mm, respectively. The distance between the centers of nearest-neighbor pores is 3.80 mm. The total length of the lattice is 19 cm. Mirror images of the pattern were etched to a depth of approximately 0.10 mm using precision sandblasting (Bancheros Glass & Etching, Inc.). Following etching, the plates were aligned and annealed in a muffle furnace. The resulting total volume of the voids (pores + throats) was approximately  $1.6 \text{ cm}^3$  and the porosity was 0.44.

At the beginning of each experiment the air in the initially empty micromodel was displaced by pressurized carbon dioxide (which is more water-soluble than air) for approximately ten minutes in order to reduce the long-term presence of trapped gas bubbles. Deionized water was then pumped into the micromodel at a low flow rate until all the gas was displaced and the pores and throats were com-

pletely filled with water. Subsequently, the water flow was turned off and trichloroethylene (TCE), which is a typical organic groundwater contaminant with density  $1.46 \text{ g/cm}^3$  at  $20^\circ\text{C}$  [16] and viscosity  $0.545 \text{ mPa s}$  at  $25^\circ\text{C}$  [17], was pumped into the micromodel until nearly all the water was displaced. The interfacial tension between TCE and water is  $0.0345 \text{ N/m}$  [18]. The TCE contained catalytic amounts of organic dye (Oil Blue N) to facilitate visualization. Oil Blue N is insoluble in water. Once the micromodel was filled with TCE, the flow of organic fluid was stopped and a gravity feed system, described below, was used to push deionized water through the micromodel at a constant pressure drop (typically 700 Pa). The resulting water flow rate through the micromodel increased slowly with time as ganglia were mobilized and displaced, thereby increasing the permeability. Over the course of a typical experiment, the average volumetric flow rate of water was  $0.08 \text{ ml/min}$ , which corresponds to a mean residence time of 20 min.

In order to ensure that a constant pressure drop was maintained across the flow cell and to eliminate pulses associated with fluid pumping, a gravity-driven fluid feed system was used during the water flood portion of the experiment. A Masterflex peristaltic cartridge pump was used to deliver degassed deionized water from a sealed reservoir to a filled 140 ml flask suspended over a shallow overflow box, thereby maintaining a constant height free surface at the top of the flask. A 1/8-inch tube (TYGON) was used to carry water from the flask to the feed port of the micromodel. A similar tube carried effluent from the exit port of the micromodel to a collection vessel. Because the volumetric flow rates used in these studies are low, the only portion of the exit tube that is continuously and completely filled with effluent is the region between the exit port and the location where the tube reaches its maximum elevation. In the remaining portion of the exit tube the fluid flows drop-wise as it empties into the

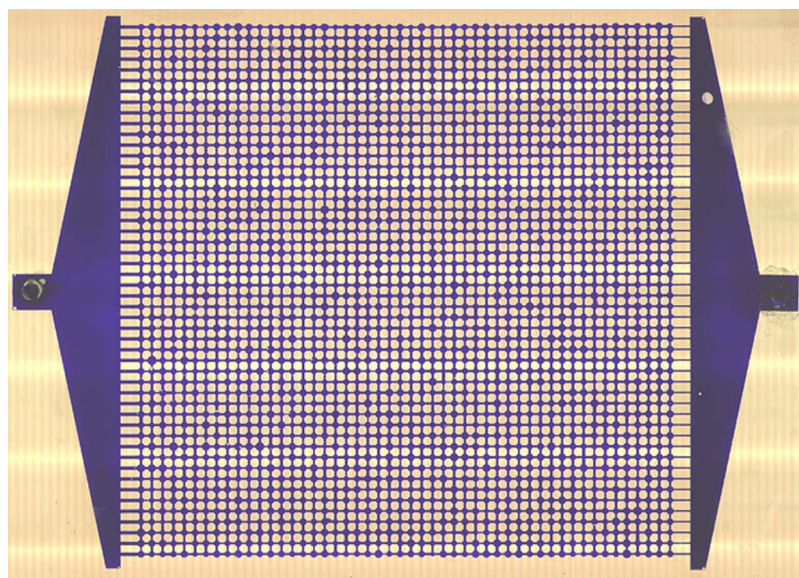


Fig. 3. Photograph of the two-dimensional micromodel filled with dyed TCE.

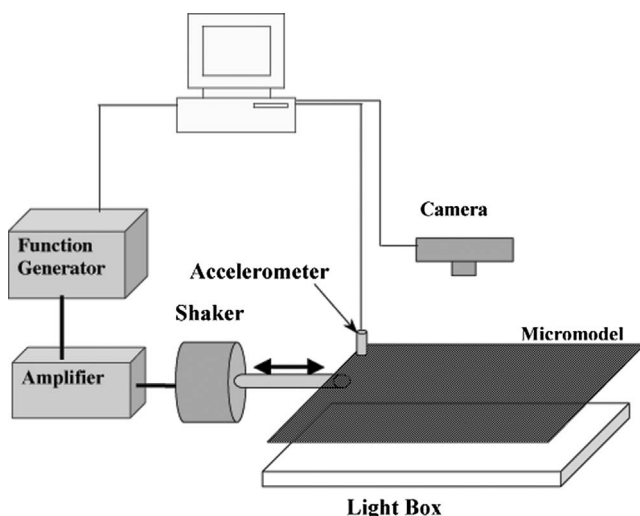


Fig. 4. Schematic of experimental apparatus layout.

effluent collection vessel. As a consequence of this design, flow through the micromodel is driven by a constant pressure gradient that is determined by the difference between the elevations of the free surface at the top of the feed flask and the highest point in the exit tube. Hence, the constant pressure driving force can easily be manipulated by simply changing the relative elevations of the feed flask and the maximum exit tube height.

The displacement of TCE by water was monitored using an optical imaging system. Specifically, a Canon PowerShot A40 color digital camera connected to a PC was mounted on a stage directly above the micromodel, as shown schematically in Fig. 4. Captured images of the micromodel have a resolution of  $1200 \times 1600$  pixels. Uniform illumination of the micromodel was provided by 5000 K light transmitted from a light box (CL-5000M, CABIN) mounted approximately two inches underneath the horizontal micromodel. The image-analysis software Image-Pro Plus 4.5.1 was used to calculate the fractional area of pores and throats occupied by the dye-containing TCE. In a typical no-vibration experiment, the TCE reached a constant residual saturation of approximately 15% of the pore/throat area within 300 h after commencing the water flood.

Horizontal vibration of the micromodel parallel to the imposed external pressure gradient was carried out using a Bruel & Kjaer vibration exciter (Type 4809). The micromodel was mounted in a Teflon-sleeved frame (which allowed the glass micromodel to translate smoothly), and the assembly was connected to the vibration exciter shaft. The displacement amplitude and the frequency of the vibration exciter shaft was controlled by a function generator (Phillips PM5134) and a power amplifier (Bruel & Kjaer, Type 2706). The resulting acceleration amplitude of the micromodel was measured using an Industrial Monitoring Instrumentation accelerometer (Model 326A02). In addition, a pressure transducer (Cole Parmer) placed upstream of the micromodel was used to measure the water inlet pressure.

### 3. Results and discussion

#### 3.1. Estimation of conditions for ganglia entrapment

Using the general form of the Laplace equation for non-spherical menisci, the maximum difference in capillary pressure along a trapped ganglion in the micromodel can be estimated as  $P_c^{\text{right}} - P_c^{\text{left}} = \sigma(1/R^{\text{throat}} - 1/R^{\text{pore}}) = 61 \text{ Pa}$ , where  $\sigma$  is the TCE/water interfacial tension and  $R^{\text{throat}}$  and  $R^{\text{pore}}$  are the respective mean radii. The typical length of entrapped ganglia in the absence of vibrations was observed to be approximately four lattice units, therefore the capillary-pressure gradient trapping the ganglia was approximately  $61 \text{ Pa}/(4 \times 0.0038 \text{ m}) = 4.0 \times 10^3 \text{ N/m}^3$ . Since all experiments were conducted under a 700 Pa total external pressure drop, the pressure gradient exerted on ganglia by the water was on average only approximately  $700 \text{ Pa}/0.19 \text{ m} = 3.7 \times 10^3 \text{ N/m}^3$ , which was less than the value necessary to mobilize the ganglia. Based upon these calculations, it is possible to estimate the magnitude of the equivalent oscillatory body force  $\rho_f a_0$  needed to mobilize trapped fluid in the micromodel if the experiment were conducted with vibration. In particular, the maximum oscillatory body force exerted on the TCE ganglia would be  $0.73 \times 10^3 \text{ N/m}^3$  for an acceleration amplitude of  $0.5 \text{ m/s}^2$ , which would result in a combined total forcing of  $4.4 \times 10^3 \text{ N/m}^3$ , which would exceed the threshold to overcome the resistive capillary force. Hence, vibration experiments were performed using acceleration amplitudes of at least  $0.5 \text{ m/s}^2$ .

#### 3.2. Repeatability of experiments

Three water flood experiments were performed in the absence of vibration until the TCE reached a constant residual saturation, as shown in Fig. 5. The overall trends of the three curves are similar, especially during the initial stages of displacement, but they become more divergent as they approach asymptotic residual saturation ( $\sim 10$ – $20\%$  of the initial TCE volume fraction). These differences are probably attributable to statistical fluctuations associated with the lattice size (only  $50 \times 50$  nodes). In particular, the residual saturation will depend sensitively upon the initial percolation pathways.

Three experimental runs were also conducted at a vibration frequency of 10 Hz and acceleration amplitude of  $3.5 \text{ m/s}^2$  from the time the water was introduced into the micromodel until the TCE in the micromodel reached residual saturation. Fig. 6 shows the normalized area of the residual TCE as a function of time for these three experiments. The repeatability for these conditions is excellent and better than that found for the no-vibration case. Because the vibratory forcing acts on all parts of the micromodel simultaneously and without discrimination, the likelihood of developing percolation pathways that bypass large portions of the flow cell (thereby leading to larger fluctuations from one experiment to the next) is diminished.

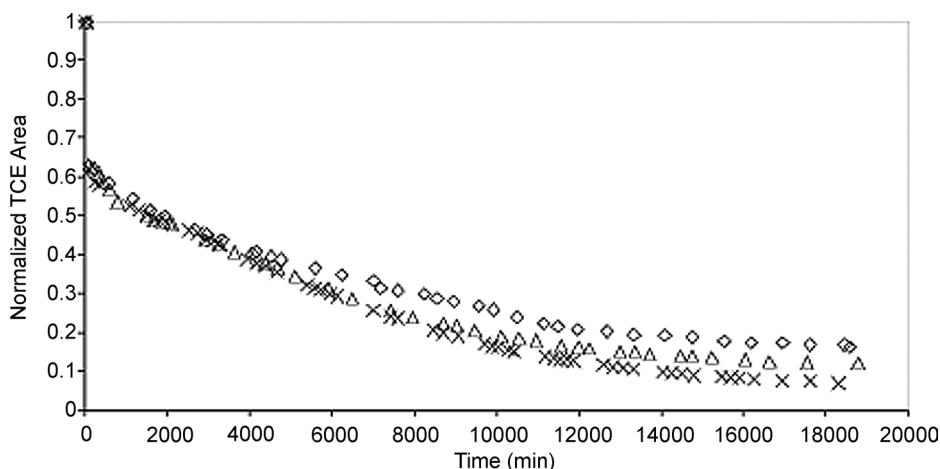


Fig. 5. Measured TCE area (normalized by initial TCE area equal to the total void area) versus time for three repeated experiments with no vibration.

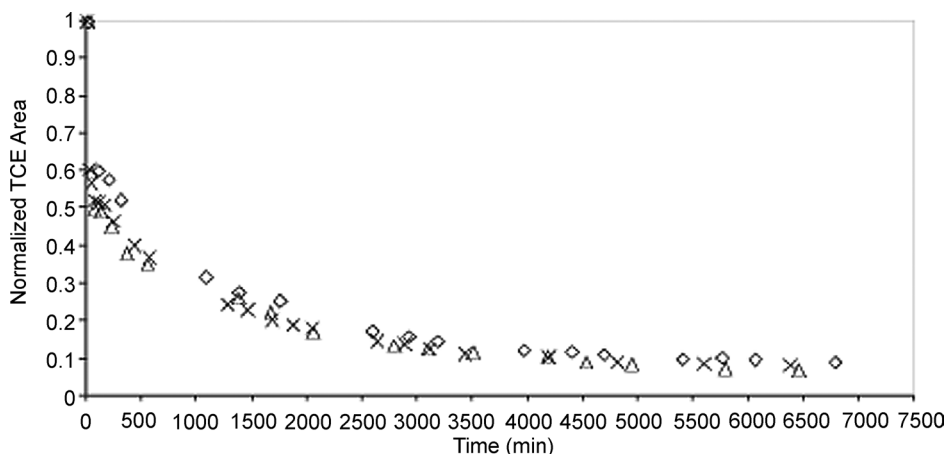


Fig. 6. Measured TCE area (normalized by initial TCE area) versus time for three repeated experiments with vibration frequency of 10 Hz and acceleration amplitude of  $3.5 \text{ m/s}^2$ .

### 3.3. Frequency effect

Experiments under vibration were carried out at a constant acceleration amplitude of  $3.5 \text{ m/s}^2$  and at frequencies of 10, 30, 60 Hz, to discern the effect of vibration frequency on ganglia mobilization. The order of magnitude of the ganglion response time in the experiment can be estimated as  $\tau \approx 10^3 \text{ kg/m}^3 \times (10^{-3} \text{ m})^2 / 10^{-3} \text{ Pa s} = 1 \text{ s}$ , showing that both of the mechanisms of the frequency dependence of the mobilization outlined in the Introduction are operational under the conditions of the experiment. Frequencies lower than 10 Hz were not investigated because, for fixed acceleration amplitude, the required displacement amplitude increases according to the inverse relation  $a_x \propto 1/f^2$ , where  $f$  is the frequency, which results in displacement amplitudes outside the range of capability of the shaker.

Results are presented in Fig. 7, which shows the normalized residual TCE area as a function of time. Also plotted are the results for the no-vibration case. In all cases with vibration, the TCE area declined much quicker and reached a lower asymptotic residual saturation than for the case with

no vibrations. Furthermore, an inverse dependence of TCE removal rate on the frequency was observed, as anticipated by the capillary-physics mechanism outlined earlier, with the highest rate occurring at the lowest frequency (10 Hz). Moreover, the difference between the TCE displacement curves for the experiments carried out at 30 and 60 Hz was not as large as the difference between the curves for the 10 and 30 Hz cases, which can be understood recalling that the vibration periods in the former two cases were already much smaller relative to the ganglion response time, explaining the inefficiency of vibrations at such high frequencies.

### 3.4. Acceleration amplitude effect

Three experiments at a fixed vibration frequency of 30 Hz were performed for acceleration amplitudes of 0.5, 1.8, 3.5, and  $5.0 \text{ m/s}^2$ . Plots of normalized TCE area as a function of time for these experiments, as well as for the no-vibration case are shown in Fig. 8. It can be seen that as the acceleration amplitude is increased, the rate of displacement of TCE increases and the asymptotic TCE residual saturation

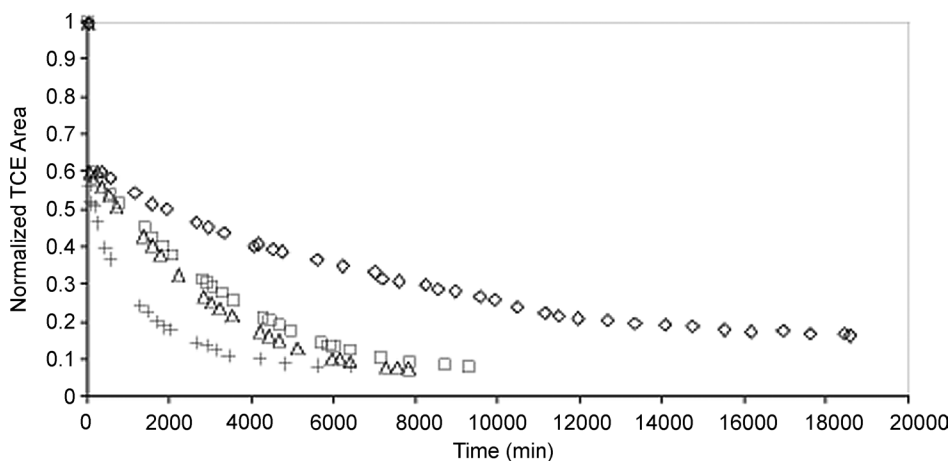


Fig. 7. Normalized TCE area versus time for experiments carried out at different vibration frequencies but at constant acceleration amplitude ( $3.5 \text{ m/s}^2$ ). Also plotted for comparison is the result for the case with no vibration. ( $\diamond$ ) No vibration, (+) 10 Hz, ( $\Delta$ ) 30 Hz, ( $\square$ ) 60 Hz.

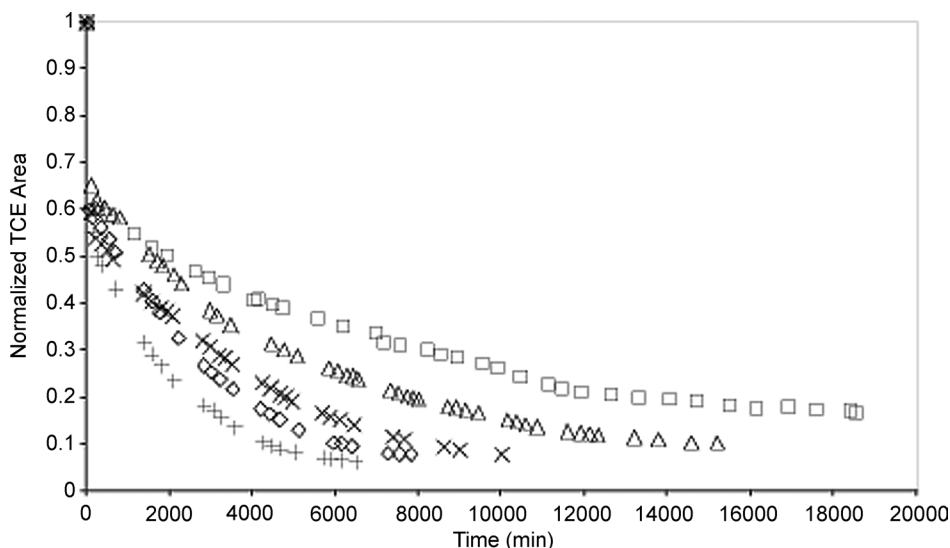


Fig. 8. Normalized TCE area versus time for experiments carried out at different acceleration amplitudes but at constant vibration frequency (30 Hz). Also plotted for comparison is the result for the case with no vibration. ( $\square$ ) No vibration, ( $\Delta$ )  $0.5 \text{ m/s}^2$ , ( $\times$ )  $1.8 \text{ m/s}^2$ , ( $\diamond$ )  $3.5 \text{ m/s}^2$ , (+)  $5.0 \text{ m/s}^2$ .

drops, as predicted by the capillary-physics mechanism. It also appears that as the acceleration amplitude is increased, eventually no further decreases in the residual saturation will be observed. As was discussed above, based upon the mean pore and throat diameters, the minimum acceleration amplitude needed to mobilize trapped ganglia can be estimated to be  $0.5 \text{ m/s}^2$ . The experimental result for this acceleration amplitude is consistent with this prediction.

#### 4. Summary

Quasi-two-dimensional glass-micromodel experiments were carried out to validate predictions of a capillary-physics mechanism of organic-ganglia mobilization under the influence of low-frequency vibrations. For fixed acceleration amplitude, TCE is more quickly displaced in a water flood experiment as the vibration frequency decreases from 60 to

10 Hz. For fixed vibration frequency, TCE displacement is more efficient as the acceleration amplitude was increased from  $0.5$  to  $5.0 \text{ m/s}^2$ . These findings are consistent with trends predicted by the capillary-physics mechanism.

The increase in the rate of TCE production proportional to the amplitude and inversely proportional to the frequency is explained by the vibrations preventing the entrapment of ganglia at any given instant of time: ganglia that would have been trapped in a non-aided flow are able to overcome the capillary barrier due to the nudging effect when the system undergoes vibrations.

Additional studies are necessary to generalize these findings before low frequency vibratory stimulation can be employed reliably in the field. In particular, experiments need to be carried out for more realistic pore and throat dimensions and converging–diverging pore geometries typically found in oil reservoirs. Also, the effects of fluid and solid properties, as well as interfacial and wetting characteristics, need to

be elucidated. However, the results of this work demonstrate that even a model based upon a simplified representation of the pore scale phenomena can provide significant insight into the behavior of more complicated systems and can be used to verify underlying physics.

### Acknowledgments

This work was supported by the National Science Foundation award EAR-0125214 and the Department of Energy award DE-FC26-01BC15165. The authors thank J. Adin Mann for providing the function generator, amplifier and vibrator used in this work, and W. Pennington and R. Turpening for stimulating discussions.

### References

- [1] Handbook on In Situ Treatment of Hazardous Waste Contaminated Soils, Environmental Protection Agency, Washington, DC, 1990, EPA/540/2-90/002.
- [2] M. Oostrom, C. Hofstee, R.C. Walker, J.H. Dane, J. Contam. Hydrol. 37 (1999) 179.
- [3] J.C. Fountain, A. Klimek, M.G. Beikirch, T.M. Middleton, J. Hazard. Mater. 28 (1991) 295.
- [4] K.D. Pennell, M. Jin, L.M. Abriola, G.A. Pope, J. Contam. Hydrol. 16 (1994) 35.
- [5] J.W. Jawitz, D.P. Dai, P.S.C. Rao, M.D. Annable, R.D. Rhue, Environ. Sci. Technol. 37 (9) (2003) 1983.
- [6] K.R. Reddy, R.E. Saichek, J. Environ. Eng. ASCE 129 (4) (2003) 336.
- [7] R. Iyer, Particulate Sci. Technol. 19 (3) (2001) 219.
- [8] I.A. Beresnev, P.A. Johnson, Geophysics 59 (6) (1994) 1000.
- [9] L.N. Reddi, S. Challa, J. Environ. Eng. ASCE 120 (5) (1994) 1170.
- [10] P.M. Roberts, I.B. Esipov, E.L. Majer, Leading Edge 22 (5) (2003) 448.
- [11] P.M. Roberts, A. Sharma, V. Uddameri, M. Monagle, D.E. Dale, L.K. Steck, Environ. Eng. Sci. 18 (2) (2001) 67.
- [12] D.R. Graham, J.J.L. Higdon, J. Fluid Mech. 425 (2000) 55.
- [13] P.P. Iassonov, I.A. Beresnev, J. Geophys. Res. B 108 (3) (2003) 2138.
- [14] M.A. Biot, J. Acoust. Soc. Am. 28 (1956) 179.
- [15] R.W. Johnson, The Handbook of Fluid Dynamics, CRC Press, 1998, pp. 9–11.
- [16] R.L. David, CRC Handbook of Chemistry and Physics, 79th ed., CRC Press, Washington, DC, 1998–1999, pp. 3–164.
- [17] R.L. David, CRC Handbook of Chemistry and Physics, 79th ed., CRC Press, Washington, DC, 1998–1999, pp. 6–170.
- [18] G. Weiss, Hazardous Chemicals Data Book, second ed., Noyes Data Corporation, Park Ridge, NJ, 1986, p. 974.